Ivo SENJANOVIĆ
Nikola VLADIMIR
Marko TOMIĆ

Effective Stiffness of the Engine Room Structure in Large Container Ships

Original scientific paper

Very large container ships are rather flexible due to the large deck openings. Therefore, hydroelastic stress analysis is required as a basis for a reliable structural design. In the early design stage, the coupling of the beam model with a 3D hydrodynamic model is rational and preferable. The calculation is performed using the modal superposition method, so natural hull modes have to be determined in a reliable way. Therefore, the advanced thin-walled girder theory, which takes the influence of shear on both bending and torsion into account, is applied for calculating the hull flexural and torsional stiffness properties. A characteristic of very large container ships is the quite short engine room, whose closed structure behaves as an open hold structure with increased torsional stiffness due to the deck effect. The paper deals with the calculation of its effective torsional stiffness parameters by utilizing the energy balance approach. Also, estimation of distortion of transverse bulkheads, as a result of torsion and warping, is given. The procedure is checked by the 3D FEM analysis of a ship-like pontoon. Such a modified beam model of the engine room structure can be included in the general beam model of a ship hull for the need of hydroelastic analysis, where only a few first natural frequencies and mode shapes are required. For practical use in the preliminary design stage of ship structures, the simplicity of the beam model presents an advantage over 3D FEM models.

Keywords: *container ship, engine room structure, torsion, warping, distortion, thin-walled girder, analytical solution, FEM, hydroelasticity*

Efektivna krutost konstrukcije strojarnice velikih kontejnerskih brodova

Izvorni znanstveni rad

Veliki kontejnerski brodovi podložni su uvijanju zbog relativno male torzijske krutosti kao posljedica velikih palubnih otvora. Stoga je provođenje hidroelastične analize nužno kao osnova za racionalno i pouzdano projektiranje konstrukcije. U ranoj fazi osnivanja preferira se sprezanje grednog strukturnog modela s 3D hidrodinamičkim modelom. Proračun se provodi metodom superpozicije prirodnih oblika vibriranja te proračun prirodnih vibracija u zraku treba biti pouzdan. Stoga je usavršena teorija tankostijenih nosača primijenjena za proračun fleksijske i torzijske krutosti, koja uzima u obzir i utjecaj smika na uvijanje. Jedna od značajki velikih kontejnerskih brodova je relativno kratka strojarnica, tako da se njena zatvorena konstrukcija ponaša kao otvorena konstrukcija teretnog skladišta povećane torzijske krutosti uslijed utjecaja paluba. U članku se razmatra određivanje efektivnih parametara krutosti koristeći energetski pristup. Također, procjenjuje se distorzija poprečnih pregrada strojarnice uslijed uvijanja i vitoperenja poprečnog presjeka. Postupak je provjeren 3D MKE analizom pontona sličnog brodskoj konstrukciji. Ovako modificirani model konstrukcije strojarnice može se jednostavno uključiti u opći gredni model brodskog trupa za potrebe hidroelastične analize, za koju je potrebno odrediti nekoliko prvih prirodnih frekvencija i oblika vibriranja. Jednostavnost grednog modela daje određenu prednost u preliminarnom projektiranju brodske konstrukcije pred upotrebom 3D MKE modela.

Ključne riječi: *kontejnerski brod, konstrukcija strojarnice, uvijanje, vitoperenje, distorzija, tankostijeni nosač, analitičko rješenje, MKE, hidroelastičnost*

Authors' Address (Adresa autora):
University of Zagreb,
Faculty of Mechanical Engineering and Naval Architecture,
I. Lučića 5, 10000 Zagreb, Croatia
E-mail: ivo.senjanovic@fsb.hr

1 Introduction

Increase in sea transport requires building of very large container ships (VLCS) [1]. Due to their flexibility, the conventional strength analysis based on rigid body wave load is not reliable enough [2, 3]. These ships have to be submitted to hydroelastic analysis and in the early design stage coupling of FEM beam structural model with 3D hydrodynamic model is a reasonable choice [4, 5].

Hydroelastic analysis is performed by the modal superposition method [6]. Thus, the beam structural model has to be sufficiently reliable to describe the ship hull dry natural modes equally well as the 3D FEM model does. For this purpose, the advanced theory of thin-walled girder is used to determine the

bending and shear stiffness, and torsional and warping stiffness with shear influence [7, 8, 9].

In medium-size container ships there are only a couple of transverse bulkheads that resist hull distortion. Hull torsion, and consequently cross-section warping, is reduced with stools integrated at the top of transverse bulkheads. The stools are modelled as discretisized restrain elements [10, 11, 12, 13, 14].

In the case of large container ships the transverse bulkheads are quite robust. The height of their girders is equal to the frame spacing, i.e. ca. 2 m. Thus, the transverse bulkheads together with the stools resist hull distortion and consequently reduce hull torsion. Due to their large number, continuous influence can be assumed through the increased value of the St. Venant torsional stiffness proportionally to the bulkhead strain energy and the open hull strain energy [15].

Another problem related to large container ships is a relatively short engine room structure which is not completely effective. Its complex deformation is illustrated in case of a 11400 TEU container ship, Figure 1, [16]. The deck shear deformation is predominant, while the stool on the hold transverse bulkheads is exposed to bending. Due to the short engine room, its transverse bulkheads are skewed but somewhat less pronouncedly than the warping of the hold bulkheads. Warping of the transom is negligible, and that is an important fact when specifying boundary conditions.
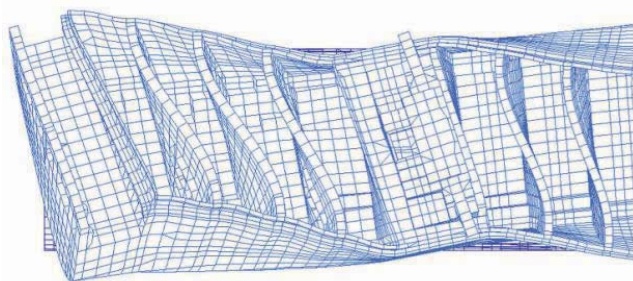

Figure 1 **Twist angle of open box girder with closed ends**
a – (B_w, ψ') compatibility
b – (B_w, ψ') discontinuity
c – effective stiffness
d – FEM
Slika 1 **Kut uvijanja otvorenog kutijastog nosača sa zatvorenim krajevima**
a – (B_w, ψ') kompatibilnost
b – (B_w, ψ') diskontinuitet
c – efektivna krutost
d – FEM

A couple of problems arise in the beam modelling of container ship structures: connection of the closed fore and aft peaks, and the closed engine room with the open holds and accounting for the effect of transverse bulkheads. Due to different vertical position of the shear centre, coupling between torsion and horizontal bending exists within displacements and sectional forces; $Y^* = Y^\circ + \psi\left(z_{SC}^* - z_{SC}^\circ\right)$, $T^\circ = T^* + Q\left(z_{SC}^* - z_{SC}^\circ\right)$, where Y is deflection, ψ is twist angle, T is torque and Q is shear force, z_{sc} is coordinate of shear centre, while $(.)^*$ and $(.)^\circ$ designate closed and open cross-section. Warping compatibility in the joint of the open and closed cross-section presents another problem which can be solved in one of the following three ways:

a. Equilibrium of bimoments, B_w, and compatibility of twist angle derivatives, ψ', [17].

b. Discontinuity of twist angle derivatives $\psi'\left(x^+\right) = s_1\psi'\left(x^-\right)$, and coupling between bending angles and twist angle $\varphi\left(x^+\right) = \varphi\left(x^-\right) + s_2\psi'\left(x^-\right)$; equilibrium of bending moments and bimoments $B_w\left(x^-\right) = s_1 B_w\left(x^+\right) - s_2 M\left(x\right)$, where s_1 and s_2 are the warping compatibility factors which depend on warping function, [10, 11].

Efficiency of the above joint conditions is illustrated in the case of a prismatic pontoon with an open middle part and closed ends: $L \times B \times H = 2.4 \times 0.4 \times 0.2$ m, $l_{cl} + l_{op} + l_{cl} = 0.6 + 1.2 + 0.6$ m, $t = 3$ mm [12]. The pontoon is exposed to the end torques of 1 kNm. The obtained twist angles for the above two compatibility conditions, as well as the third one based on the effective stiffness determined by the theory of elasticity [18], are correlated in Figure 2. The third solution is the closest one to the 3D FEM results [17] and therefore it is preferable for the practical use due to the reason of simplicity.
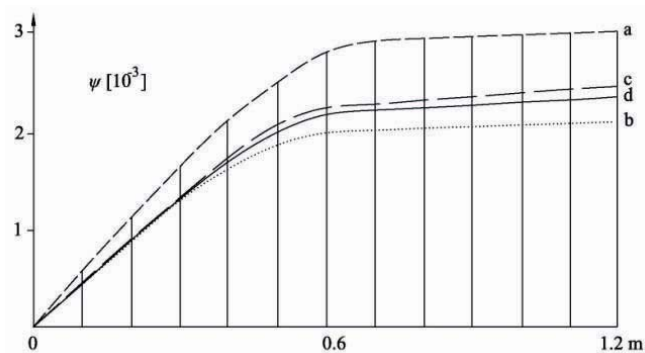

Figure 2 **Bird's-eye view of the 11400 TEU container ship aftbody, the 5th natural mode**
Slika 2 **Ptičji pogled na krmu kontejnerskog broda od 11400 TEU, peti oblik prirodnih vibracija**

This paper aims to determine the effective values of stiffness parameters of a short engine room structure in the beam model, utilizing the energy approach. Due to the small aspect ratio, length/breadth, the engine room structure behaves as an open hold structure with increased torsional stiffness. Therefore, torsionally induced horizontal bending is small and can be neglected, which makes the determination of the effective values of torsional stiffness parameters much easier. In addition, distortion of the engine room transverse bulkheads is considered based on the known torsional and warping response. The basic formulae of the thin-walled girder theory are used and the procedure is verified by a 3D FEM analysis of a ship-like pontoon.

2 Outline of the thin-walled girder theory

In the thin-walled girder theory, it is assumed that the structure behaves as a membrane and that there is no distortion of the cross-section [10, 11, 12, 13, 19, 20]. Also, in the advanced theory shear influence on torsion is taken into account similarly as in the flexural beam theory [7, 8]. As a result, there is analogy between bending and torsion.

The twist angle consists of a pure twist angle and a shear contribution

$$\psi = \psi_t + \psi_s, \tag{1}$$

where the latter is

$$\psi_s = -\frac{EI_w}{GI_s}\frac{d^2\psi_t}{dx^2}. \tag{2}$$

E and G are Young's modulus and shear modulus, while I_w and I_s are warping modulus and shear moment of inertia, respectively.

The girder sectional torque consists of a pure torsional part and a warping contribution [14]

$$T = T_t + T_w, \ T_t = GI_t\frac{d\psi_t}{dx},$$
$$T_w = GI_s\frac{d\psi_s}{dx} = -EI_w\frac{d^3\psi_t}{dx^3}. \tag{3}$$

The torques T_t and T_w are the result of shear stress τ_t and τ_w due to pure torsion and fixed ends against warping, respectively. Constrained warping also causes normal stress

$$\sigma = Ew\frac{d^2\psi_t}{dx^2}, \tag{4}$$

where w is the warping function (relative axial displacement due to unit torsional deformation ψ_t'). The normal stress distribution per cross-section is condensed in the warping bimoment, which represents the stress work on the relative displacement w

$$B_w = \int_s \sigma tw\,ds = EI_w\frac{d^2\psi_t}{dx^2}, \tag{5}$$
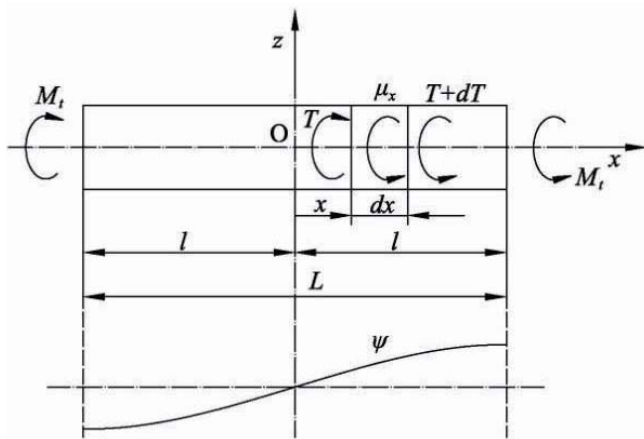
where

$$I_w = \int_s w^2 t\,ds. \tag{6}$$

Figure 3 **Girder torsion**
Slika 3 **Uvijanje nosača**

The equilibrium of the total sectional torque with the distributed external load, $dT = -\mu_x dx$, leads to the differential equation, Figure 3

$$EI_w\frac{d^4\psi_t}{dx^4} - GI_t\frac{d^2\psi_t}{dx^2} = \mu_x. \tag{7}$$

Its solution reads

$$\psi_t = A_0 + A_1\frac{x}{l} + A_2\text{ch}\alpha x + A_3\text{sh}\alpha x + \psi_p, \tag{8}$$

where

$$\alpha = \sqrt{\frac{GI_t}{EI_w}} \tag{9}$$

and ψ_p is a particular solution. Thus, the total twist angle (1) takes the following form

$$\psi = A_0 + A_1\frac{x}{l} + A_2\left(1-\frac{I_t}{I_s}\right)\text{ch}\alpha x + A_3\left(1-\frac{I_t}{I_s}\right)\text{sh}\alpha x + \psi_p - \frac{EI_w}{GI_s}\psi_\pi''. \tag{10}$$

Now, it is possible to derive formulae for the cross section warping and sectional moments, Equations (3) and (5)

$$u = w\frac{d\psi_t}{dx} = w\left(\frac{A_1}{l} + A_2\alpha\text{sh}\alpha x + A_3\alpha\text{ch}\alpha x + \psi_p'\right), \tag{11}$$

$$T_t = GI_t\left(\frac{A_1}{l} + A_2\alpha\text{sh}\alpha x + A_3\alpha\text{ch}\alpha x + \psi_p'\right), \tag{12}$$

$$T_w = -GI_t\left(A_2\alpha\text{sh}\alpha x + A_3\alpha\text{ch}\alpha x\right) - EI_w\psi_p''', \tag{13}$$

$$T = GI_t\left(\frac{A_1}{l} + \psi_p'\right) - EI_w\psi_p''', \tag{14}$$

$$B_w = GI_t\left(A_2\text{ch}\alpha x + A_3\text{sh}\alpha x\right) + EI_w\psi_p''. \tag{15}$$

3 Torsion of prismatic girder

The girder is loaded with torque M_t at the ends, while $\mu_x = 0$. The ends are fixed against warping. The twist angle is an anti-symmetric function and therefore constants $A_0 = A_2 = 0$. The remaining constants A_1 and A_3 are determined by satisfying the relevant boundary conditions

$$x = l, \ T = M_t, \ u = 0. \tag{16}$$

Thus, one finds that

$$A_1 = \frac{M_t l}{GI_t}, \ A_3 = -\frac{M_t l}{GI_t}\frac{1}{\alpha l\text{ch}\alpha l}. \tag{17}$$

Displacements and forces, Equations (10)… (15), take the following form:

$$\psi = \frac{M_t l}{GI_t}\left[\frac{x}{l} - \left(1-\frac{I_t}{I_s}\right)\frac{\text{sh}\alpha x}{\alpha l\text{ch}\alpha l}\right], \tag{18}$$

$$u = \frac{M_t}{GI_t}\left(1 - \frac{\text{ch}\alpha x}{\text{ch}\alpha l}\right)w, \tag{19}$$

$$T_t = M_t\left(1 - \frac{\text{ch}\alpha x}{\text{ch}\alpha l}\right), \tag{20}$$

$$T_w = M_t \frac{\text{ch}\alpha x}{\text{ch}\alpha l}, \tag{21}$$

$$B_w = -M_t \frac{\text{sh}\alpha x}{\alpha \text{ch}\alpha l}. \tag{22}$$
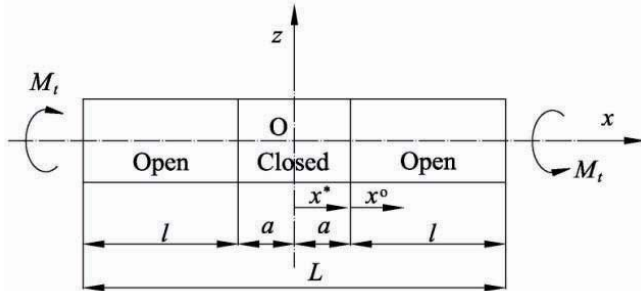
4 Torsion of segmented girder

Figure 4 Torsion of segmented girder
Slika 4   **Uvijanje segmentnog nosača**

Let us consider a girder consisting of three segments, Figure 4. The second segment is located in the middle so that the girder is symmetric. The girder load and the boundary conditions are the same as in the previous case, Section 3. Each segment is specified in its local coordinate system, Figure 4. The properties of the middle and end segments are designated by (*) and (°), and symbols A_i and B_i are used for the integration constants, respectively. Constants A_0 and A_2 are zero because of antisymmetric deformation.

The compatibility conditions at the segment joint and the boundary conditions are the following:

$$\psi^*(a) = \psi^\circ(0), \ \psi_t^{*\prime}(a) = \varepsilon \psi_t^{\circ\prime}(0),$$
$$T^*(a) = T^\circ(0), \ B_w^*(a) = \eta B_w^\circ(0), \tag{23}$$
$$u^\circ(l^\circ) = 0, \ T^\circ(l^\circ) = M_t.$$

The warping compatibility factors, ε and η, are introduced in order to make handle of all three sets of joint conditions specified in the Introduction, possible, i.e. Points a and b, case $s_2 \neq 0$ and $s_2 = 0$.

From the third and last conditions (23) one finds

$$A_1 = \frac{M_t a}{GI_t^*}, \ B_1 = \frac{M_t l^\circ}{GI_t^\circ}. \tag{24}$$

The remaining four conditions (23) lead to the following system of algebraic equations:

$$\begin{bmatrix} \alpha\text{ch}\alpha a & 0 & -\varepsilon\beta \\ I_t^*\text{sh}\alpha a & -hI_t^\circ & 0 \\ 0 & \beta\text{sh}\beta l^\circ & \beta\text{ch}\beta l^\circ \end{bmatrix} \begin{Bmatrix} A_3 \\ B_2 \\ B_3 \end{Bmatrix} = \frac{M_t}{G} \begin{Bmatrix} \dfrac{\varepsilon}{I_t^\circ} - \dfrac{1}{I_t^*} \\ 0 \\ -\dfrac{1}{I_t^\circ} \end{Bmatrix}, \tag{25}$$

$$B_0 = A_1 + A_3\left(1 - \frac{I_t^*}{I_s^*}\right)\text{sh}\alpha a - B_2\left(1 - \frac{I_t^\circ}{I_s^\circ}\right), \tag{26}$$

where

$$\alpha = \sqrt{\frac{GI_t^*}{EI_w^*}}, \ \beta = \sqrt{\frac{GI_t^\circ}{EI_w^\circ}}. \tag{27}$$

The solution of the system (25) reads

$$A_3 = \frac{D_{A3}}{D}, \ B_2 = \frac{D_{B2}}{D}, \ B_3 = \frac{D_{B3}}{D}, \tag{28}$$

where

$$D_{A3} = \frac{M_t\eta}{G}\left[\left(\varepsilon - \frac{I_t^\circ}{I_t^*}\right)\text{ch}\beta l^\circ - \varepsilon\right],$$

$$D_{B2} = -\frac{M_t}{G}\text{sh}\alpha a\left[\left(1 - \frac{\varepsilon I_t^*}{I_t^\circ}\right)\text{ch}\beta l^\circ + \frac{\varepsilon I_t^*}{I_t^\circ}\right], \tag{29}$$

$$D_{B3} = \frac{M_t}{G}\left[\left(1 - \frac{\varepsilon I_t^*}{I_t^\circ}\right)\text{sh}\alpha a \ \text{sh}\beta l^\circ - \frac{\eta\alpha}{\beta}\text{ch}\alpha a\right],$$

$$D = \eta I_t^\circ \alpha\text{ch}\alpha a \ \text{ch}\beta l^\circ + \varepsilon I_t^*\beta\text{sh}\alpha a \ \text{sh}\beta l^\circ.$$

5 Stiffness of engine room structure

Container ship hull is rather weak against torsion due to large deck openings [10, 11, 12, 13]. The engine room is quite short, the aspect ratio length/breadth is ca. 1:2. Therefore, the hold double skin is continued through the engine room to ensure that the warping and bending stresses have a continuous stress flow through the transverse bulkheads surrounding the engine room. The upper deck in the large cross-section warping field is exposed to boundary shear load, while the double bottom rotates around the vertical axis as a "rigid body", Figure 2. Thus, the shear deformation of the lower decks in the engine room is decreasing from the upper deck to the bottom.

Due to the above facts, the relevant stiffness parameters of the engine room closed cross-section are not fully effective. Therefore, it can be assumed, as in the case of transverse bulkheads [15] that the effective warping modulus and the shear inertia modulus are equal to those of the open cross-section (without decks), i.e. $\tilde{I}_w \approx I_w^\circ$ and $\tilde{I}_s \approx I_s^\circ$ respectively, while only the torsional modulus is increased due to the decks influence. Its value is somewhere between those of the open and closed cross-section, depending on the decks aspect ration, $I_t^\circ < \tilde{I}_t < I_t^*$.

The equivalent torsional modulus $\tilde{I}_t$ can be determined by the energy approach and presented in the form

$$\tilde{I}_t = (1 + C)I_t^\circ, \tag{30}$$

where C is the ratio of the decks strain energy and the strain energy of the corresponding hull portion without decks.

The relative axial displacement of the upper deck boundaries, with respect to the double bottom, is the result of their warping, Eq. (11)

$$U = |U_D| + |U_B| = (|w_D| + |w_B|)\psi_t'. \tag{31}$$

It causes deck in-plane (membrane) deformation. The problem can be solved in an approximate analytical way by considering the deck as a beam. Its horizontal anti-symmetric deflection consists of pure bending and shear contribution, Figure 5.
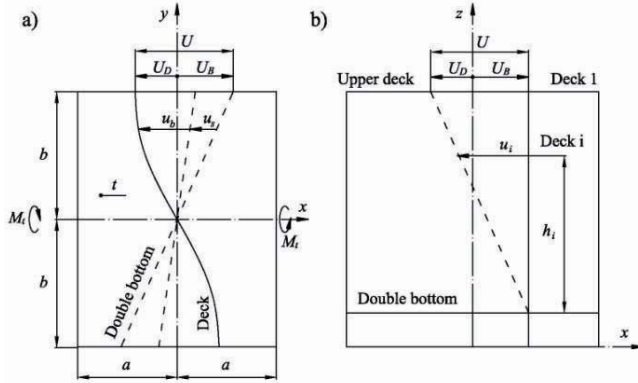

Figure 5 **Upper deck deformation and double bottom rotation**
a – bird's-eye view
b – lateral view
Slika 5 **Deformacija gornje palube i zakretanje dvodna**
a – ptičji pogled
b – bočni pogled

The former is assumed in the form

$$u_b = \frac{y}{2b}\left[3-\left(\frac{y}{b}\right)^2\right]U_b, \tag{32}$$

which satisfies the relevant boundary conditions: $u_b\,(0)$ and $u_b''(0)=0$, where U_b is the boundary bending deflection. Shear deflection depends on bending deflection

$$u_s = -\frac{EI}{GA}\frac{\mathrm{d}^2 u_b}{\mathrm{d}y^2} = 2(1+v)\left(\frac{a}{b}\right)^2\frac{y}{b}U_b, \tag{33}$$

where deck cross-section area, $A = 2at$, its moment of inertia, $I = \frac{2}{3}a^3 t$, and the relation $E = 2(1+v)G$ are taken into account, Figure 5. The total deflection is obtained by summing up Eqs. (32) and (33), i.e. $u = u_b + u_s$. The relation between the total boundary deflection and the bending boundary deflection reads

$$U = \left[1 + 2(1+v)\left(\frac{a}{b}\right)^2\right]U_b. \tag{34}$$

The total deck strain energy consists of the bending and shear contribution

$$E_1 = \frac{1}{2}EI\int_{-b}^{b}\left(\frac{\mathrm{d}^2 u_b}{\mathrm{d}y^2}\right)^2\mathrm{d}y + \frac{1}{2}GA\int_{-b}^{b}\left(\frac{\mathrm{d}u_s}{\mathrm{d}y}\right)^2\mathrm{d}y. \tag{35}$$

By substituting Eqs. (32), (33) and (34) into Eq. (35), we obtain

$$E_1 = \frac{4(1+v)Gt\left(\frac{a}{b}\right)^3}{1+2(1+v)\left(\frac{a}{b}\right)^2}U^2 \tag{36}$$

On the other hand, the strain energy of the engine room hull portion, without decks and transverse bulkheads, reads

$$E_H = \frac{1}{2}\int_{-a}^{a}T_t\psi_t'\mathrm{d}x = GI_t^\circ a\psi_t'^2, \tag{37}$$

where T_t is specified in Eqs. (3) and for ψ_t' the constant value within a short span $2a$, is assumed. Finally, by taking the strain energy of all decks into account as well as Eq. (31), one finds for coefficient C in Eq. (30)

$$C = \frac{\sum E_i}{E_H} = \frac{4(1+v)t_1\left(\frac{a}{b}\right)^3\left(|w_D|+|w_B|\right)^2 k}{\left[1+2(1+v)\left(\frac{a}{b}\right)^2\right]I_t^\circ a}, \tag{38}$$

where

$$k = \sum\frac{V_i}{V_1}\left(\frac{h_i}{h_1}\right)^2 \tag{39}$$

is the sum of the deck influence coefficients. It is obtained by assuming that their strain energy is proportional to the volume, V, and deformation is linearly increasing with the deck distance from the inner bottom, h, Figure 5.

In spite of the high deck aspect ratio, ca. 1:2, the applied beam theory for determining the deck in-plane deformation gives quite good results. Performing an FEM analysis with the deck membrane model showed that the beam model is only 6% stiffer than the FEM model.

6 Distortion of segmented pontoon

The open and closed cross-section segments are connected at the transverse bulkhead, which is subjected to distortion due to different shear flows on its front and back side, induced by the torque M_t, Figure 6. The shear flow of the open cross-section, s°, is parabolic, while that of the closed cross-section, s^* is uniform. The resulting side forces are $S_S = S_S^\circ - S_S^*$, and the deck and bottom forces read $S_D = S_D^*$ and $S_B = S_B^*$, since $S_D^\circ = 0$ for the open section and $S_B^\circ = 0$ due to self equilibrium for the given bottom flow s°, Figure 6. The above shear forces satisfy the static equilibrium conditions. The internal stress equilibrium leads to the distortion of the transverse bulkhead, δ.

The shear flows shown in Figure 6 are realistic for the long open and closed pontoon segments. However, in case of short closed segment, as the engine room structure, the deck is weakly effective and its shear flow is considerably reduced, Figure 7. As a result, the remained part of the cross-section behaves similarly to the open one. Difference of the shear flows, $s^\circ - s^*$, is quite small but still causes bulkhead distortion, δ, which can be estimated in the following way.
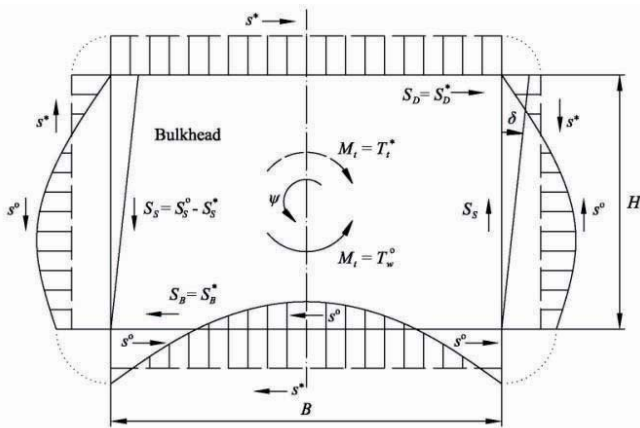
Figure 6   **Shear forces at the joint of open and closed cross-section segments**
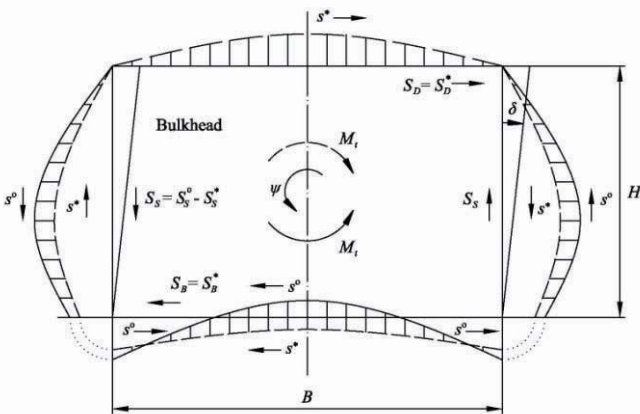Slika 6   **Smične sile na spoju otvorenog i zatvorenog segmenta**

Figure 7   **Shear forces at the joint of long open and short closed cross-section segments (qualitative presentation)**
Slika 7   **Smične sile na spoju dugog otvorenog i kratkog zatvorenog segmenta (kvalitativni prikaz)**

Tendency of the deck and double bottom of the engine room structure subjected to torsion is rotation around the vertical

Figure 8   **Deck and bulkhead displacements and in-plane deformations**
Slika 8   **Pomaci i membranske deformacije palube i pregrade**
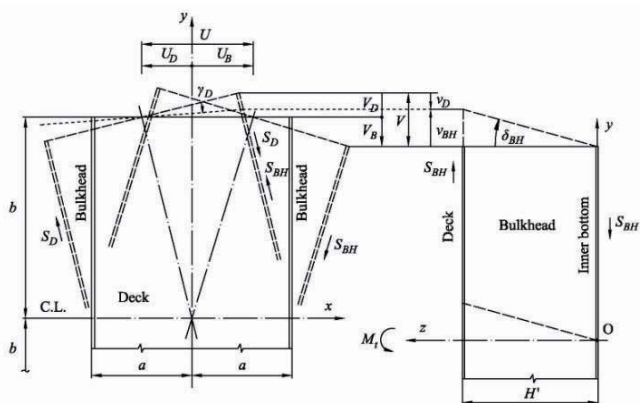
axis in the opposite directions due to warping of cross-sections, Figure 8.

The total transverse gap between the deck corner and the bulkhead top yields, Figure 8

$$V = V_D + V_B = \frac{a}{b}U, \tag{40}$$

where relative axial deck displacement with respect to double bottom, U, is given by Eq. (31). Gap V is cancelled by the deck corner transverse displacement v_D and the bulkhead top displacement v_{BH} in the opposite directions, as a result of equilibrated internal shear forces S_D and S_{BH}, Figure 8. The shear forces depend on the shear deformations $\gamma_D = v_D/a$ and $\delta_{BH} = v_{BH}/H'$, respectively, where δ_{BH} is distortional angle, Figure 8. Thus, one can write for the deck shear force

$$S_D = 2Gt_1 k \frac{b}{a} v_D, \tag{41}$$

where t_1 is the upper deck thickness, while k takes contribution of all decks to the resulting deck force S_D into account. It is obtained by assuming a proportional increase of the deck shear deformation with the deck distance from the inner bottom, and moment equilibrium of the shear forced S_i and S_D. That gives the same definition of k as that estimated by energy balance, Eq. (39).

In the similar way, the bulkhead shear force reads

$$S_{BH} = 2Gt_{BH} \frac{b}{H'} v_{BH}. \tag{42}$$

The force equilibrium leads to the ratio of the deck and bulkhead transverse displacements

$$\frac{v_D}{v_{BH}} = \frac{t_{BH} a}{t_1 kH'}, \tag{43}$$

which is reciprocal to their stiffnesses. On the other hand, $v_D + v_{BH} = V$ and by taking Eqs. (31), (40) and (43) into account, one obtains

$$\delta_{BH} = \frac{v_{BH}}{H'} = \frac{\left(|w_D| + |w_B|\right)\psi'_t}{b\left(\dfrac{H'}{a} + \dfrac{t_{BH}}{t_1 k}\right)}. \tag{44}$$

If the bulkhead thickness increases, t_{BH}, the distortion angle decreases, and vice versa.

Figure 9   **Deck boxes as beams on elastic supports**
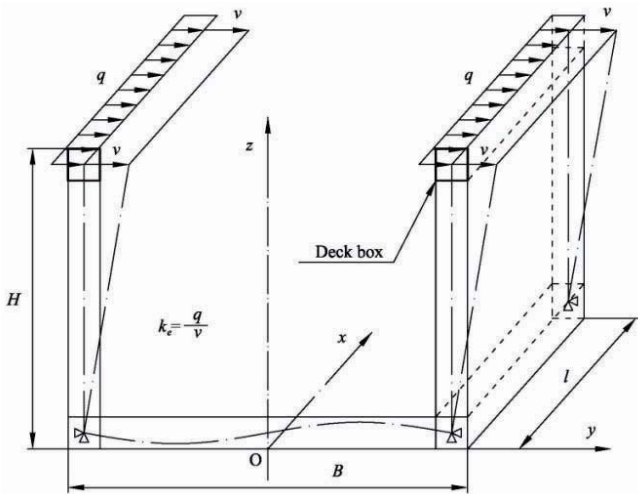Slika 9   **Palubni kutijasti nosači kao grede na elastičnoj podlozi**
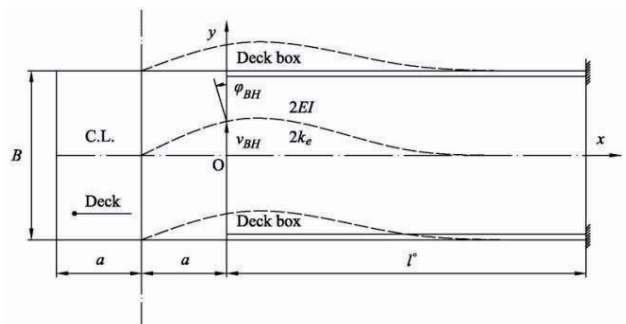
Figure 10 **Definition of deck box support stiffness**
Slika 10 **Definiranje krutosti elastične podloge palubnih nosača**

Distribution of the distortion angle δ within the engine room is almost linear. Along the open hold it causes bending of the upper deck boxes as beams on elastic supports, Figure 9 [18]. The support stiffness, k_e, is determined as the ratio of the imposed deck load, q, and the responded displacement, v, Figure 10. Two deck boxes can be considered as one girder with double bending and support stiffnesses, $2I$ and $2k_e$, respectively. Since the open hold is quite long, l_0, mutual boundary influence is negligible, and therefore only the decreasing terms of homogenous solution for the beam on elastic support can be used. By satisfying the relevant boundary conditions, Figure 9, we get

$$v = e^{-\vartheta x}\left[v_{BH}\cos\vartheta x + \left(v_{BH} + \frac{\varphi_{BH}}{\vartheta}\right)\sin\vartheta x\right], \qquad (45)$$

where

$$\vartheta = \sqrt[4]{\frac{k_e}{4EI}}, \qquad (46)$$

$\varphi_{BH} = v_{BH}/a$ while v_{BH} is founded from Eq. (44). Finally, function of distortion angle reads $\delta = v/H'$.

Based on the known deflection of the deck box, v, it is possible to determine the bending moment, $M = -EIv''$, and stress, $\sigma = My/I$, where y is the distance of a considered point on the box cross-section from the neutral line. By employing (45) one obtains

$$\sigma_b = y\sqrt{\frac{Ek_e}{I}}e^{-\vartheta x}\left[\left(v_{BH} + \frac{\varphi_{BH}}{\vartheta}\right)\cos\vartheta x - v_{BH}\sin\vartheta x\right]. \quad (47)$$

The complete stress consists of the membrane part due to restrained warping, Eq. (4), and the above bending stress, Eq. (47).

7 Geometric properties of ship-like pontoon

A 7800 TEU Container Vessel of the following main particulars is taken into consideration:

Length overall $L_{oa} = 334$ m
Length between perpendiculars $L_{pp} = 319$ m
Breadth $B = 42.8$ m
Depth $H = 24.6$ m
Draught $T = 14.5$ m
Displacement $\Delta = 135530$ t.
Material properties are the following:
Young's modulus $E = 2.06 \cdot 10^8$ kN/m²
Shear modulus $G = 0.7923 \cdot 10^8$ kN/m²
Poisson's ratio $v = 0.3$.

The ship's lateral plan and midship section are shown in [15]. The engine room is located ca. 0.2 L from the aft perpendicular, where the cross-section is reduced. However, in this numerical investigation the engine room is extended to the full midship profile so that a prismatic ship-like pontoon can be created and analysed.

The geometrical properties of the open and closed ship cross-section are determined using computer program STIFF [22] based on the strip theory of thin-walled girders [23, 24], Table 1. It is evident that the cross-section area of the closed section is 50% higher than that of the open section. Torsional modulus of the closed section is much higher than that of the open section. The shear centre of the closed section is in the middle of the cross-section, while that of the open section is below the keel.

Table 1 **Geometric properties of ship cross-sections**
Tablica 1 **Geometrijske značajke poprečnih presjeka broda**

Quantity	Symbol, unit	Open section (°)	Closed section (*)
Cross-section area	A, m²	6.394	10.200
Horizontal shear area	A_{sh}, m²	1.015	2.959
Vertical shear area	A_{sv}, m²	1.314	2.094
Vertical position of neutral line	z_{NL}, m	11.66	13.96
Vertical position of shear centre	z_{SC}, m	-13.50	9.60
Horizontal moment of inertia	I_{bh}, m⁴	1899	2331
Vertical moment of inertia	I_{bv}, m⁴	676	889
Torsional modulus	I_t, m⁴	14.45	939.5
Warping modulus	I_w, m⁶	171400	24010
Shear polar moment of inertia	I_s, m⁴	710.5	173.6

Figure 11 **Warping function of the open cross-section**
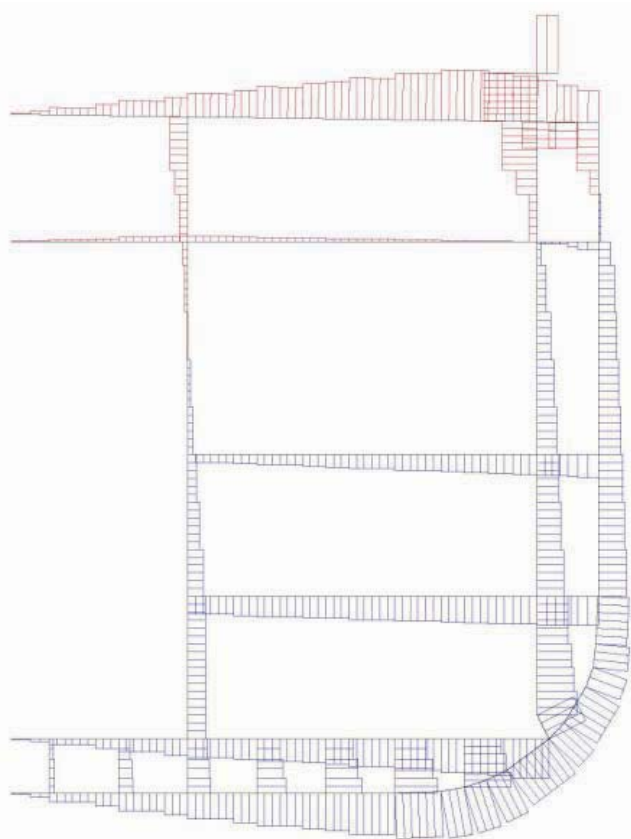Slika 11 **Vitoperenje otvorenog poprečnog presjeka**
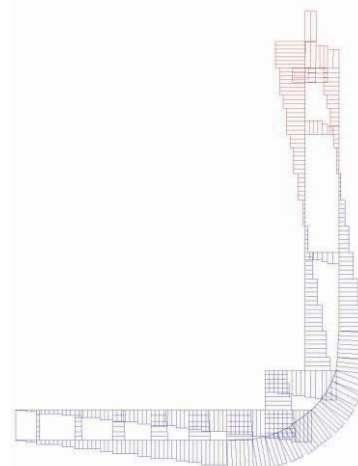
Figure 12 **Warping function of the closed cross-section**
Slika 12   **Vitoperenje zatvorenog poprečnog presjeka**

The warping functions of the open and closed cross-sections, w, are shown in Figures 11 and 12. The relative axial displacement of the inside point of the upper deck and bilge, at the level of the inner bottom, as the representative quantities, reads $w_D = -221$ m² and $w_B = 267$ m² respectively. The relative moment of inertia of the decks volume, Eq. (39), is calculated in Table 2.

Table 2   **Relative moment of inertia of deck structure volume**
Tablica 2 **Relativni moment inercije volumena konstrukcije palube**

Item i	Substructure	V_i (m³)	h_i (m)	$\frac{V_i}{V_1}\left(\frac{h_i}{h_1}\right)^2$
1	Upper deck	12.738	22.6	1
2	Deck 2	14.038	18.234	0.7174
3	Deck 3	8.955	10.422	0.1495
4	Deck 4	6.434	5.214	0.0269
				$k = 1.894$

8 Pontoon torsion

8.1 Uniform open pontoon

Torsion of the uniform pontoon of the length $L = 300$ m, with the open cross-section is considered. The stiffness parameters

are taken from Table 1. Warping at the boundaries is restrained according to Figure 2 and comments at the end of Section 1. Torsional moment $M_t = 40570$ kNm is imposed at the pontoon ends. The pontoon is considered free in the space and the problem is solved analytically in Section 3. The total twist angle $\psi = \psi_t + \psi_s$ and the derivative of the torsional contribution, ψ_t', Eqs. (18) and (19), necessary for warping determination, are shown in Figure 13.
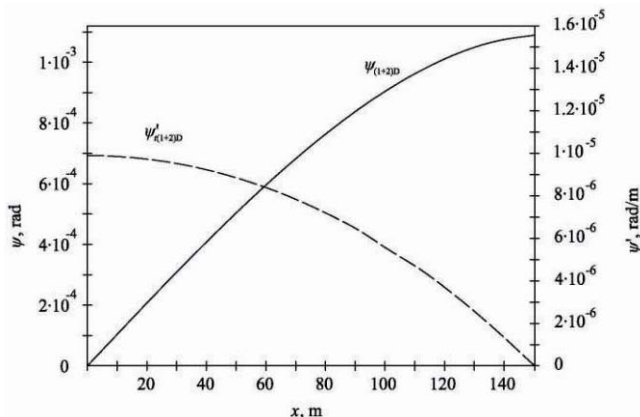

Figure 13 **Deformation functions of uniform pontoon**
Slika 13   **Funkcija deformacije jednolikog pontona**

8.2 Pontoon with a closed segment

The analytical solution for the torsion of a pontoon consisting of three segments is presented in Section 4, where compatibility factors for the conventional compatibility conditions (a) are used $\varepsilon = \eta = 1$. The length of the middle closed segment is $2a = 20.2$ m. The geometrical parameters of the open cross-sections are listed in Table 1. Diagrams of the total twist angle ψ and derivative of the pure twist angle, ψ_t', are shown in Figure 14.
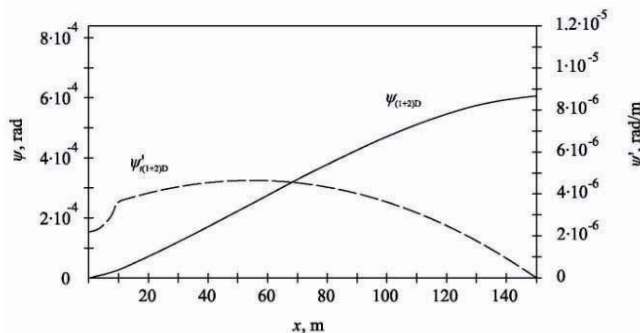

Figure 14 **Deformation functions of segmented pontoon, actual parameters**
Slika 14   **Funkcija deformacije segmentnog pontona, aktualni parametri**

8.3 Pontoon with effective parameters of a closed segment

The procedure for torsional analysis is the same as in the previous case. The reduction of the torsional modulus of the closed segment due to its shortness, i.e. deck contribution to the torsional modulus of the open section, is elaborated in Section 5.

The following values of the basic parameters are used: $a = 10.1$ m, $b = 19.17$ m, $t_1 = 0.01645$ m, $w_D = -221$ m², $w_B = 267$ m², Figures 11 and 12, I_t^o m⁴, Table 1, $k = 1.894$, Table 2. As a result $C = 22.42$, Eq. (38), and accordingly $\tilde{I}_t = 338.4$ m⁴, Eq. (30), are obtained. Since $\tilde{I}_t = 0.36 I_T^*$, the effect of the short engine room structure on its torsional stiffness is obvious.
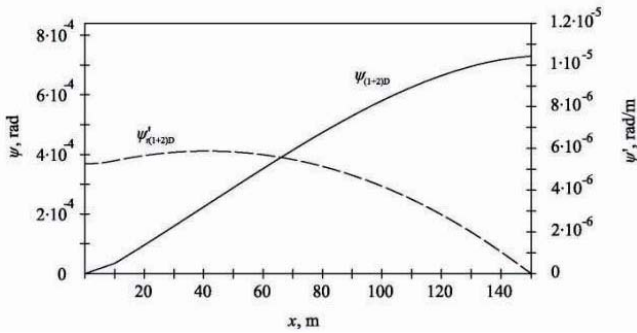

Figure 15 **Deformation functions of segmented pontoon, effective parameters**
Slika 15 **Funkcija deformacije segmentnog pontona, efektivni parametri**

The obtained pontoon deformation functions are shown in Figure 15. There are large differences between the results obtained for the actual and effective parameters, Figures 14 and 15. The maximum displacements for all three considered cases, i.e. the uniform pontoon and the segmented pontoon with actual and effective parameters, are compared in Table 3.

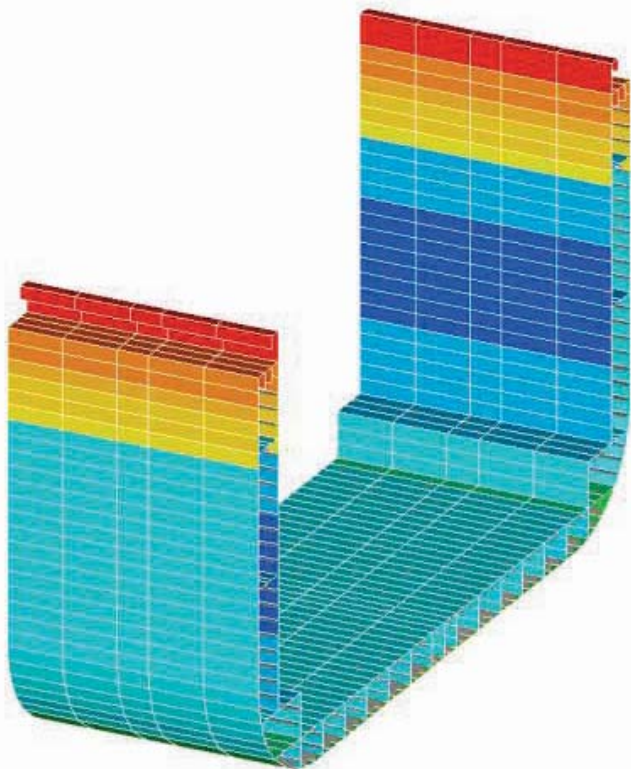Figure 16 **A typical hold superelement**
Slika 16 **Tipični superelement skladišta**

Table 3 **Pontoon displacements**
Tablica 3 **Pomaci pontona**

	Uniform pontoon	Segmented pontoon	
		Actual parameters	Effective parameters
$\psi(L/2)$, rad	0.0010893	0.0006066	0.0007331
$\psi_t'(0)$, rad	$9.897 \cdot 10^{-6}$	$2.202 \cdot 10^{-6}$	$5.306 \cdot 10^{-6}$

Distribution of distortion angle, δ, is determined by employing the procedure described in Section 6 with the following input data: $\psi_t' = 5.454 \cdot 10^{-6}$, $H' = 22.6$ m, $t_1 = 0.01645$ m, $t_{BH} = 0.01131$ m in Eq. (44); moment of inertia of the deck box cross-section $I = 0.711$ m⁴, stiffness of the elastic support $k_e = 721$ kN/m². The value of k_e is obtained by FEM for a pontoon segment, Figure 16.
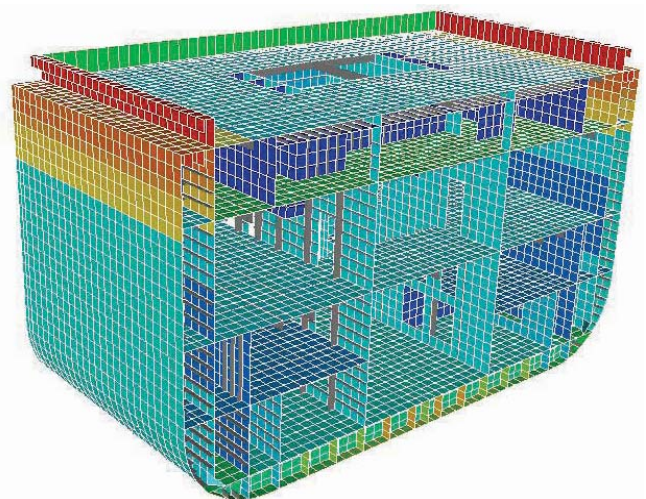
9 FEM analysis

Figure 17 **Engine room superelement**
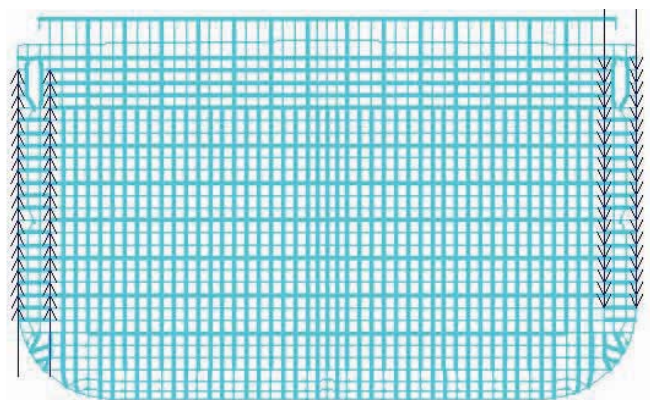Slika 17 **Superelement strojarnice**

Figure 18 **Load on the model ends**
Slika 18 **Rubno opterećenje modela**

In order to verify the numerical procedure for torsional analysis by the beam model with effective stiffness parameters, designated as (1+2)D for short, the 3D FEM models of the uniform and segmented pontoon are created using software [25].

The former consists of 22 open superelements, Figure 16, while in the latter, two central superelements are exchanged with the one engine room superelement, Figure 17. The pontoon ends are closed with transverse bulkheads. The shell finite elements are used. The pontoons are loaded at their ends with the vertical distributed forces in the opposite directions, generating total torque $M_t = 40570$ kNm, Figure 18. The midship section is fixed against the transverse and vertical displacements, and the pontoon ends are constrained against the axial displacements (warping).

Figure 19 **Deformation of uniform pontoon, lateral and bird's-eye view**
Slika 19 **Deformacije jednolikog pontona, bočni i ptičji pogled**

Figure 20 **Deformation of segmented pontoon, lateral and bird's-eye view**
Slika 20 **Deformacije segmentnog pontona, bočni i ptičji pogled**

Lateral and bird's eye views on the deformed uniform and segmented pontoon are shown in Figures 19 and 20 respectively. In the former presentation the deformation is monotonous, while in the latter one the influence of the more rigid engine room structure is evident. A detailed view of this pontoon portion is presented in Figure 21. It is apparent that the double bottom and

Figure 21 **Lateral, axial, bird's-eye and fish views on deformed engine room superelement**
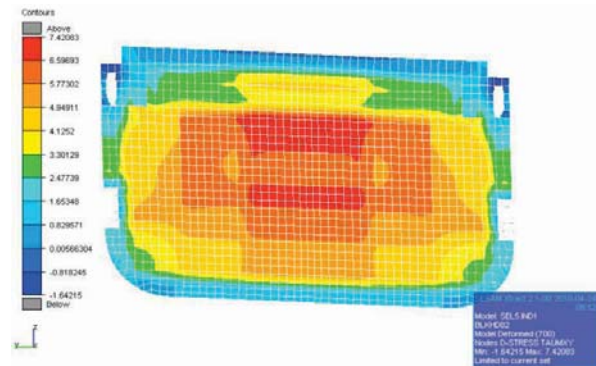Slika 21 **Bočni, uzdužni, ptičji i riblji pogled na deformirani superelement strojarnice**

Figure 22 **Shear stresses in the front engine room bulkhead**
Slika 22 **Smična naprezanja u pramčanoj pregradi strojarnice**

Figure 23 **Shear stresses at the internal boundary of the front engine room bulkhead**
Slika 23 **Smična naprezanja na unutarnjem rubu pramčane pregrade strojarnice**
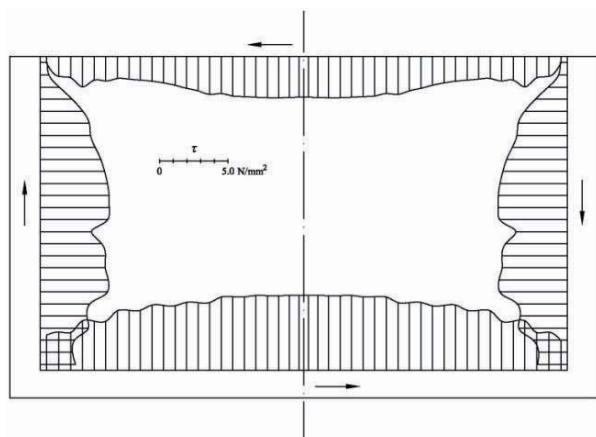
sides rotate as a "rigid body", while the decks and transverse bulkheads are exposed to shear deformation. The shear stress distribution in the front engine room bulkhead is shown in Figure 22. The boundary stresses, which cause distortion of the cross-sections, are presented in Figure 23. The assumed shear forces in the theoretical consideration of distortion, Figure 7, are similar to the actual boundary shear stress distribution in Figure 23.

10 Comparative analysis

10.1 Uniform pontoon

If one draws the twist angle diagram based on 3D FEM results, almost the same shape as that from the $(1 + 2)$D analysis is obtained, Figure 13. The ratios of the maximum displacements, in the two models, i.e. their twist angles and axial displacements, read
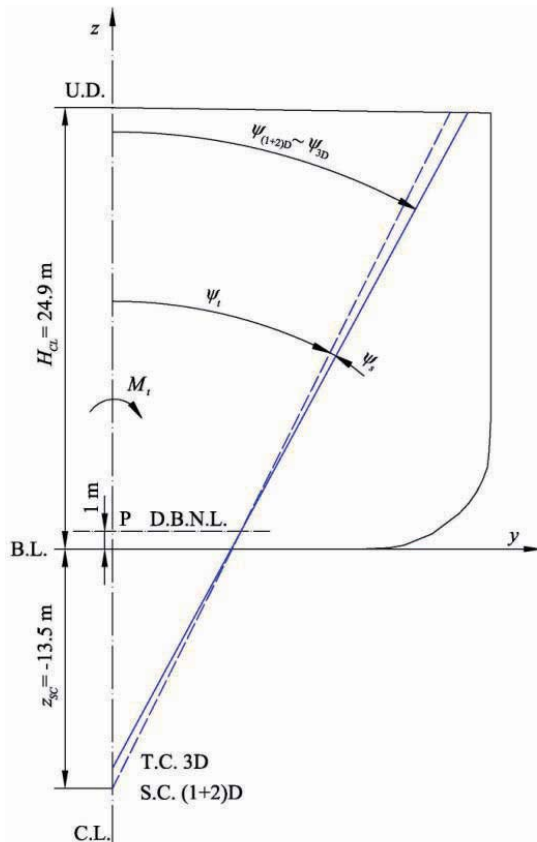
$$x = L/2: \quad \frac{\psi_{(1+2)D}}{\psi_{3D}} = \frac{0.00108934}{0.00108192} = 1.00685,$$

$$x = 0, \text{ upper deck: } \frac{u_{(1+2)D}}{u_{3D}} = \frac{-2.18718 \text{ mm}}{-2.17655 \text{ mm}} = 1.00488,$$

$$x = 0, \text{ bilge: } \frac{u_{(1+2)D}}{u_{3D}} = \frac{2.63947 \text{ mm}}{2.59264 \text{ mm}} = 1.01806.$$

Discrepancies in this simple case are within 2%, which is quite good.

Figure 24 **Twist angle at the pontoon end**
Slika 24   **Kut uvijanja na kraju pontona**

The maximum twist angles at the pontoon end are also compared in Figure 24. The total twist angle of the analytical solution, $\psi_{(1+2)D}$, is almost equal to that of the FEM analysis, ψ_{3D}. The value of $\psi_{(1+2)D}$ consists of pure torsional part ψ_t and shear contribution ψ_s. The former causes the cross-section rotation around the shear centre, S.C., while the latter continues its rotation around point P at the level of the double bottom neutral line. As a result, the twist centre is obtained, T.C. Figure 24 [15], which is not the same point as S.C.

10.2. Segmented pontoon with effective stiffness

The twist angles determined by the analytical beam solution and the FEM analysis for the pontoon bottom and side are compared in Figure 25. As can be noticed, there are some small discrepancies between $\psi_{(1+2)D,bottom}$ and $\psi_{3D,bottom}$, which are reduced to a negligible value at the pontoon ends:

$$x = L/2: \quad \frac{\psi_{(1+2)D,bottom}}{\psi_{3D,bottom}} = \frac{0.000733153}{0.000731985} = 1.0016.$$

The distortion curve of the $(1+2)$D solution, $\delta_{(1+2)D} = \psi_{(1+2)D,side} - \psi_{(1+2)D,bottom}$, also follows quite well that of the 3D FEM analysis.
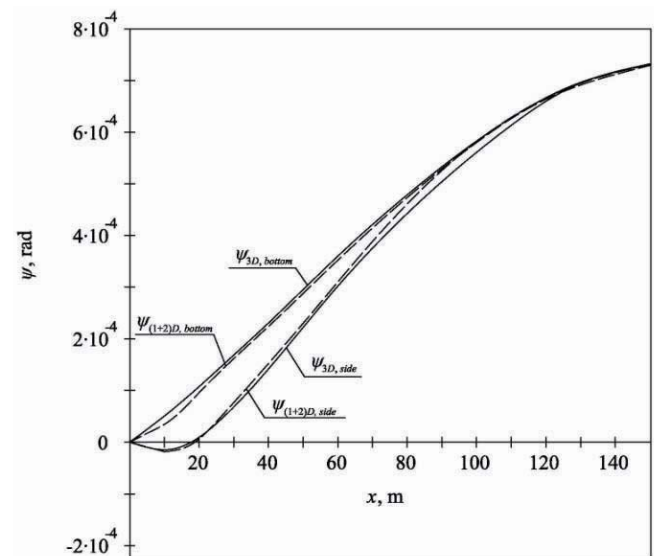

Figure 25 **Twist angles of the segmented pontoon**
Slika 25   **Kutevi uvijanja segmentnog pontona**

Warping of cross-section is evaluated by comparing axial displacements of the bilge and upper deck as representative points, Fig. 26. Correlation of the results obtained by the beam theory and FEM analysis is quite good from engineering point of view. There are some discrepancies between the axial displacements at the deck level in the engine room area as a result of large shear deformation, Figure 21. However, this is a local phenomenon, which cannot easily be captured by the beam theory.

In order to have better insight into the structural deformation, the longitudinal distribution of the vertical position of the twist centre is shown in Figure 27. Its value is somewhat reduced in
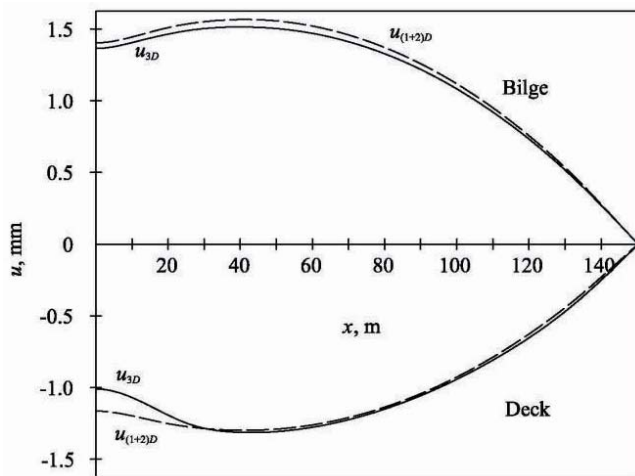
Figure 26 **Axial displacements of the deck and bottom**
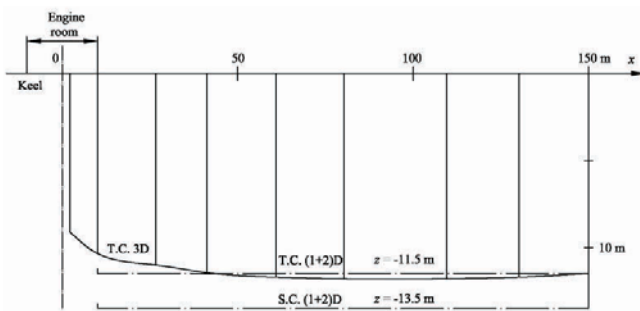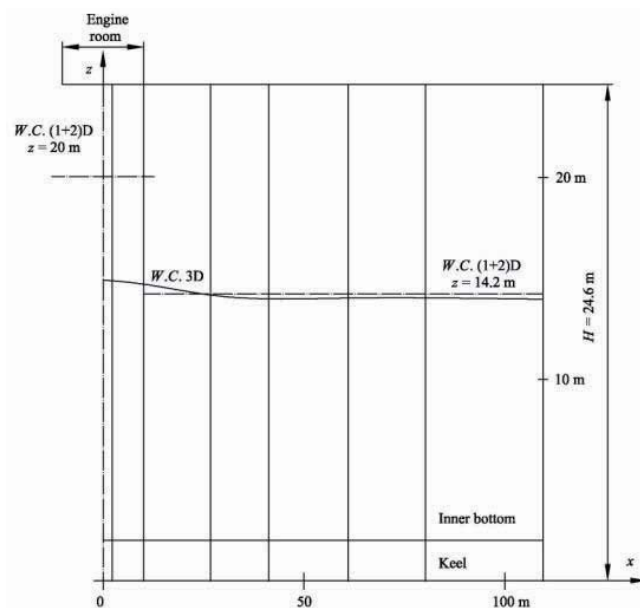Slika 26   **Uzdužni pomaci palube i dna**

Figure 27 **Vertical position of the twist centre**
Slika 27   **Vertikalni položaj centra uvijanja**

Figure 28 **Vertical position of the warping centre**
Slika 28   **Vertikalni položaj centra vitoperenja**

the engine room area, but it is still too far from the twist centre of the closed segment, which would induce considerable horizontal bending. Another criterion for recognizing bending in the torsional response is the value of the integral $I_{wy} = \int_A wy\,\mathrm{d}A$ which is zero in case of no bending. Depending on that value, the warping centre (defined as the point at the inner side shell with zero axial displacement, Figures 11 and 12) is moved from the open to the closed cross-section position, Figure 28. Since that change is quite small within the engine room area, one can conclude that horizontal bending is negligible. Based on the above facts, the introduced assumption that the short engine room structure behaves as an open one with increased torsional stiffness is acceptable.
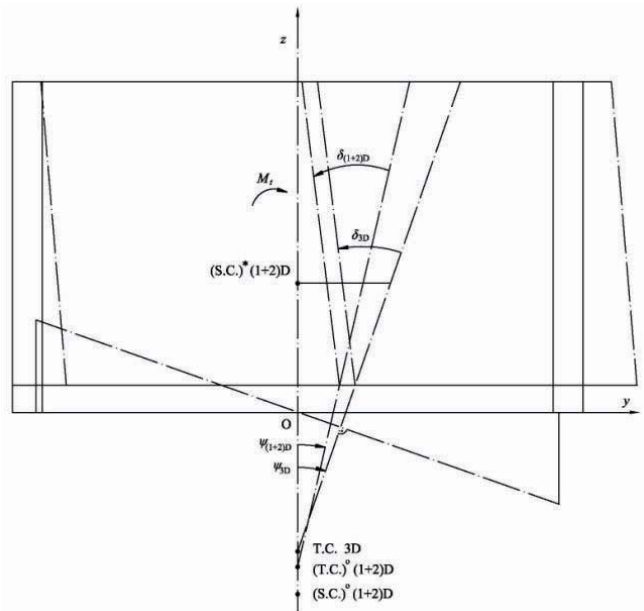

Figure 29 **Twist and distortion angles of the joint cross-section of the open and closed segments**
Slika 29   **Kutevi uvijanja i distorzije spoja otvorenog i zatvorenog segmenta**

Deformation of the joint cross-section is shown in Figure 29, where the position of the twist centres for the open and closed cross-sections is indicated and compared with the position of the twist centre for the real 3D structure. Also, the twist angles, ψ_{3D} and $\psi_{(1+2)D}$, and the distortion angle, δ, which are of the same order of magnitude, are drawn.

11 Conclusion

Hydroelastic analysis of large container ships is currently becoming a problem [26]. For reasons of simplicity, and especially in the early design stage, the beam model of the hull girder is coupled with a 3D hydrodynamic model. Transverse bulkheads increase the hull torsional modulus considerably. This problem is solved with the energy approach, considering the bulkheads as an orthotropic plate.

In this paper, a similar approach is used to determine the effective torsional stiffness parameters of the short engine room structure. It has been found that most of the strain energy is due

to the deck in-plane bending and shear deformation caused by the hull cross-section warping. The deck deformation increases with its distance from the double bottom, which mainly rotates as a "rigid body". By modelling the deck as a beam with shear influence on deflection, the problem is simplified and focused on the determination of the deck plating volume.

Pontoon distortion is a result of different shear flow distributions of the open and closed pontoon segments connected at the engine room bulkheads. In the considered case, distortion does not have a big influence on torsion, and therefore it is estimated in addition as the second step of calculation, based on the torsional results. Distortion is reduced by increasing the bulkhead thickness.

Adoption of closed cross-section stiffness moduli and the satisfaction of compatibility conditions at the joint of the closed engine room segment with the hold structure of the open cross-section presents a real problem, related to the application of the beam model of a ship hull. The offered solution for the engine room structure modelling is quite simple and its correlation with the 3D FEM results in the case of ship-like pontoon shows acceptable agreement. Therefore, it can be generally used for improving the beam structural model in a hydroelastic analysis of relatively flexible ships such as large container vessels. Due to variable cross-section properties, the beam finite element method is preferable.

Acknowledgment

References

[1]   PAYER, H.: "Technological and economic implications of mega-container carriers", SNAME Transactions, Vol. 109 (2001), p. 101-120.

[2]   VALSGÅRD, S., SVENSEN, T.E., THORKILDSEN, H.: "A computational method for analysis of container vessels, SNAME Transactions, Vol. 103 (1995), p. 371-393.

[3]   SHI, B., LIU, D., WIERNICKI, C.: "Dynamic loading approach for structural evaluation of ultra large container carriers", SNAME Transactions, 113 (2005), p. 402-417.

[4]   MALENICA, Š., SENJANOVIĆ, I., TOMAŠEVIĆ, S., STUMPF, E.: "Some aspects of hydroelastic issues in the design of ultra large container ships", The 22nd International Workshop on Water Waves and Floating Bodies, IWWWFB, Plitvice Lakes, Croatia; 2007.

[5]   TOMAŠEVIĆ, S.: "Hydroelastic model of dynamic response of container ships in waves" (in Croatian), Ph.D. Thesis, University of Zagreb, Zagreb, 2007.

[6]   BISHOP, R.E.D., PRICE, W.G.: "Hydroelasticity of Ships", Cambridge University Press, 1979.

[7]   PAVAZZA, R.: "Bending and torsion of thin-walled beams of open section on elastic foundation", Ph.D. Thesis (in Croatian). University of Zagreb, Zagreb, 1991.

[8]   PAVAZZA, R.: "Introduction to thin-walled girder analysis" (in Croatian) University of Split, 2007.

[9]   PAVAZZA, R.: "Torsion of thin-walled beams of open cross-section with influence of shear", International Journal of Mechanical Sciences. 2005, 47, p. 1099-1122.

[10] HASLUM, K., TONNESSEN, A.: "An analysis of torsion in ship hulls", European Shipbuilding, 1972; 5/6, p. 67-89.

[11] PEDERSEN, P.T.: "A beam model for the torsional-bending response of ship hulls", RINA Transactions, 1983, p.171-182.

[12] PEDERSEN, P.T.: "Torsional response of containerships". Journal of Ship Research, 1985; 29, p. 194-205.

[13] STENEROTH, E.R, ULFVARSON, A.Y.J.: "The snaking of open ships", International Shipbuilding Progress, 1976, 23 257, p. 3-9.

[14] PAVAZZA, R., PLAZIBAT, B., MATOKOVIĆ, A.: "Idealisation of ships with large hatch openings by a thin-walled rod of open section on many elastic supports", Thin-Walled Structures 1998, 32, p. 305-325.

[15] SENJANOVIĆ, I., TOMAŠEVIĆ, S., RUDAN, S., SENJANOVIĆ, T.: "Role of transverse bulkheads in hull stiffness of large container ships", Engineering Structures 2008; 30(9), p. 2492-2509.

[16] URŠIĆ, J.: "Ship Strength II, (in Croatian), University of Zagreb, Zagreb, 1983.

[17] SENJANOVIĆ, I., FAN, Y.: "Pontoon torsional strength analysis related to ships with large deck openings", Journal of Ship Research, 1991; 35(4), p. 339-351.

[18] SENJANOVIĆ I., FAN, Y.: "On torsional and warping stiffness of thin-walled girders", Thin-Walled Structures, 1991, 11, p. 233-276.

[19] SENJANOVIĆ, I., TOMAŠEVIĆ, S., VLADIMIR, N.: "An advanced theory of thin-walled girders with application to ship vibrations", Marine Structures (2009), 22: p. 387-437.

[20] VLASOV, V.Z.: "Thin-walled elastic beams", Israel Program for Scientific Translation Ltd, Jerusalem, 1961.

[21] SENJANOVIĆ, I.: "One solution of the torsion problem on container ships, Part I and II, (in Croatian), Brodogradnja 1972, 23(1,2)

[22] …: "STIFF", User's Manual. FAMENA, Zagreb, 1990.

[23] SENJANOVIĆ, I., FAN, Y.: "A higher-order theory of thin-walled girders with application to ship structures", Computers & Structures 1992; 43(1):31-52.

[24] SENJANOVIĆ, I., Fan, Y.: "A finite element formulation of ship cross-sectional stiffness parameters", Brodogradnja; 41(1993)1, p. 27-36.

[25] ...: "SESAM", User's Manual. Det Norske Veritas, Høvik; 2007.

[26] …"Proceedings of International Conference on Design & Operation of Container Ships", RINA, London; 2006.

Nomenclature

A	– cross-section area
A_c	– common cross-section area
A_i, B_i	– integration constants
a	– one half of engine room length
B_w	– warping bimoment
C	– energy coefficient
D	– determinant
E	– Young's modulus
E_i	– strain energy
G	– shear modulus
I_s, I_t, I_w	– beam shear, torsional and warping moduli
L	– beam and pontoon length
l	– segment length
M_t	– external torque
s	– contour coordinate
s_1, s_2	– compatibility factors
T	– torque
T_t, T_w	– twisting and warping torques
t	– plate thickness
u	– axial displacement
w	– warping function
x,y,z	– coordinates
$z_{S.C.}$	– ordinate of shear centre
$\alpha_i, \beta, \vartheta$	– coefficients of function arguments
δ	– distortion angle
ε, η	– compatibility factors
μ	– distributed torque
υ	– Poisson's ratio
σ	– normal stress
ψ	– twist angle
ψ'	– twist deformation
$(^o)$	– open section
$(^*)$	– closed section
$(^\square)$	– effective value